Emergence of Majorana and Dirac Particles in Ultracold Fermions via Tunable Interactions, Spin-Orbit Effects, and Zeeman Fields

Kangjun Seo, Li Han, and C. A. R. Sá de Melo
School of Physics, Georgia Institute of Technology, Atlanta, Georgia 30332, USA
(Received 30 December 2011; published 6 September 2012)

We discuss the emergence of rings of zero-energy excitations in momentum space for superfluid phases of ultracold fermions when spin-orbit effects, Zeeman fields, and interactions are varied. We show that phases containing rings of nodes possess nontrivial topological invariants, and that phase transitions between distinct topological phases belong to the Lifshitz class. Upon crossing phase boundaries, existing massless Dirac fermions in the gapless phase annihilate to produce bulk zero-mode Majorana fermions at phase boundaries, and then become massive Dirac fermions in the gapped phase. We characterize these tunable topological phase transitions via several spectroscopic properties, including excitation spectrum, spectral function, and momentum distribution.

DOI: 10.1103/PhysRevLett.109.105303 PACS numbers: 67.85.Lm, 03.75.Ss

Ultracold atoms have now become standard laboratories to test for existing or new theoretical ideas in atomic, condensed matter, nuclear, and astrophysics. The major appeal found in these table-top experiments is the ability to tune interactions, populations, species of atoms, and dimensionality—which constitute the standard toolbox for investigations of interacting bosonic or fermionic systems. Very recently, a new tool was added to the toolbox: the ability to tune simultaneously spin-orbit (SO) and Zeeman fields in a system of ultracold bosonic atoms [1]. The same tool can also be used to study ultracold fermionic atoms [1–3], and to simulate different condensed matter systems such as topological insulators [4], noncentrosymmetric superconductors [5], and nonequilibrium systems [6], where SO coupling of the Rashba type [7] is encountered.

This direct connection to condensed matter physics inspired a new direction in ultracold fermionic atoms where SO coupling of the Rashba type has been investigated very recently [8–13]. However, SO fields currently realized in experiments involving ultracold atoms correspond to an equal superposition of Rashba [7] $\mathbf{h}_{\rm R}(\mathbf{k}) = v_{\rm R}(-k_y\hat{\mathbf{x}} + k_x\hat{\mathbf{y}})$ and Dresselhaus [14] $\mathbf{h}_{\rm D}(\mathbf{k}) = v_{\rm D}(k_y\hat{\mathbf{x}} + k_x\hat{\mathbf{y}})$ fields, leading to the equal-Rashba-Dresselhaus (ERD) form [1,13] $\mathbf{h}_{\rm ERD}(\mathbf{k}) = vk_x\hat{\mathbf{y}}$, where $v_{\rm R} = v_{\rm D} = v/2$. Other forms of SO fields require additional lasers and create further experimental difficulties [15]. The current Zeeman-SO Hamiltonian created in the laboratory is $\mathbf{H}_{\rm ZSO}(\mathbf{k}) = -h_z\sigma_z - h_y\sigma_y - h_{\rm ERD}(\mathbf{k})\sigma_y$ for an atom with center-of-mass momentum $\mathbf{k}$ and spin basis $|\uparrow\rangle, |\downarrow\rangle$. The fields $h_z = -\Omega_R/2$, $h_y = -\delta/2$, and $h_{\rm ERD}(\mathbf{k}) = vk_x$ can be controlled independently, and used to explore phase diagrams, as achieved in ^{87}Rb experiments [1]. Here, $\Omega_{\rm R}$ is the Raman coupling and δ the detuning.

In this Letter, we describe the emergence of bulk Majorana and Dirac particles in ultracold Fermi superfluids via tunable interactions, SO effects, and Zeeman fields. Furthermore, we characterize their emergence in three-dimensional systems through spectroscopic properties such as excitation spectrum, spectral function, and momentum distribution.

Hamiltonian.—We start from the Hamiltonian density $\mathcal{H}(\mathbf{r}) = \mathcal{H}_0(\mathbf{r}) + \mathcal{H}_I(\mathbf{r})$, with $\hbar = 1$. The single-particle contribution is

$$\mathcal{H}_0(\mathbf{r}) = \sum_{s,s'} \psi_s^\dagger(\mathbf{r})[\hat{K}\mathbf{1} + \mathbf{H}_{\rm ZSO}(-i\nabla)]_{ss'}\psi_{s'}(\mathbf{r}), \quad (1)$$

where $\hat{K} = -\nabla^2/2m - \mu$ and $\psi_s^\dagger(\mathbf{r})$ are the creation operators for fermions with spin s located at $\mathbf{r}$. The interaction term $\mathcal{H}_I(\mathbf{r}) = -g\psi_\uparrow^\dagger(\mathbf{r})\psi_\downarrow^\dagger(\mathbf{r})\psi_\downarrow(\mathbf{r})\psi_\uparrow(\mathbf{r})$ is local, and g represents the strength of the contact interaction. We define the total number of fermions as $N = N_\uparrow + N_\downarrow$, and the induced population imbalance as $P_{\rm ind} = (N_\uparrow - N_\downarrow)/N$. We choose our scales through the Fermi momentum k_F defined from $N/V = k_F^3/(3\pi^2)$, leading to the Fermi energy $\epsilon_F = k_F^2/2m$ and Fermi velocity $v_F = k_F/m$.

We focus on the zero-detuning case $\delta = 0$ ($h_y = 0$), use the basis $|\mathbf{k}, s\rangle \equiv \psi_s^\dagger(\mathbf{k})|0\rangle$, where $|0\rangle$ is the vacuum state, and write $\mathcal{H}_0(\mathbf{r})$ in momentum space as the matrix $\mathbf{H}_0(\mathbf{k}) = K(\mathbf{k})\mathbf{1} - h_z\sigma_z - h_{\rm ERD}(\mathbf{k})\sigma_y$, where $K(\mathbf{k}) = \mathbf{k}^2/2m - \mu$. The interaction Hamiltonian $\mathcal{H}_I(\mathbf{r})$ can also be converted into momentum space as $\mathcal{H}_I(\mathbf{q}) = -gb^\dagger(\mathbf{q})b(\mathbf{q})$, where the pair creation operator $b^\dagger(\mathbf{q}) = \sum_{\mathbf{k}} \psi_\uparrow^\dagger(\mathbf{k}_+)\psi_\downarrow^\dagger(\mathbf{k}_-)$ with $\mathbf{k}_\pm = \pm\mathbf{k} + \mathbf{q}/2$ and g can be expressed in terms of the scattering length a_s through $V/g = -Vm/(4\pi a_s) + \sum_{\mathbf{k}} 1/(2\epsilon_{\mathbf{k}})$.

Helicity basis.—The matrix $\mathbf{H}_0(\mathbf{k})$ can be diagonalized in the helicity basis $|\mathbf{k}, \alpha\rangle \equiv \Phi_\alpha^\dagger(\mathbf{k})|0\rangle$ via a momentum-dependent SU(2) rotation. The helicity spins $\alpha = \Uparrow, \Downarrow$ are aligned or antialigned with respect to the effective magnetic field $\mathbf{h}_{\rm eff}(\mathbf{k}) = h_z\hat{\mathbf{z}} + h_{\rm ERD}(\mathbf{k})\hat{\mathbf{y}}$. The eigenvalues of $\mathbf{H}_0(\mathbf{k})$ are $\xi_\Uparrow(\mathbf{k}) = K(\mathbf{k}) - |\mathbf{h}_{\rm eff}(\mathbf{k})|$ and $\xi_\Downarrow(\mathbf{k}) = K(\mathbf{k}) + |\mathbf{h}_{\rm eff}(\mathbf{k})|$. The interaction Hamiltonian $\mathcal{H}_I(\mathbf{q})$

can be written in the helicity basis as $\tilde{\mathcal{H}}_I(\mathbf{q}) = -g\sum_{\alpha\beta\gamma\delta} B^\dagger_{\alpha\beta}(\mathbf{q}) B_{\gamma\delta}(\mathbf{q})$. Pairing is now described by the operator $B^\dagger_{\alpha\beta}(\mathbf{q}) = \sum_{\mathbf{k}} \Lambda_{\alpha\beta}(\mathbf{k}_+, \mathbf{k}_-) \Phi^\dagger_\alpha(\mathbf{k}_+) \Phi^\dagger_\beta(\mathbf{k}_-)$ and its Hermitian conjugate. $\Lambda_{\alpha\beta}(\mathbf{k}_+, \mathbf{k}_-)$ is directly related to the matrix elements of the momentum-dependent SU(2) rotation into the helicity basis, and reveals that the center-of-mass momentum $\mathbf{k}_+ + \mathbf{k}_- = \mathbf{q}$ and the relative momentum $\mathbf{k}_+ - \mathbf{k}_- = 2\mathbf{k}$ are coupled and no longer independent.

Tensor order parameter.—From the expression of $B_{\alpha\beta}(\mathbf{q})$, it is clear that pairing between fermions of $\mathbf{k}_\pm$ can occur within the same helicity band (intrahelicity pairing), or between two different helicity bands (interhelicity pairing). For pairing at $\mathbf{q} = 0$, the order parameter (OP) for superfluidity is the tensor $\Delta_{\alpha\beta}(\mathbf{k}) = \Delta_0 \Lambda_{\alpha\beta}(\mathbf{k}, -\mathbf{k})$, where $\Delta_0 = -g\sum_{\gamma\delta}\langle B_{\gamma\delta}(\mathbf{0})\rangle$, leading to components $\Delta_{\Uparrow\Uparrow}(\mathbf{k}) = i\Delta_T(\mathbf{k})\mathrm{sgn}(k_x) = -\Delta_{\Downarrow\Downarrow}(\mathbf{k})$ for helicity projection $\lambda = \pm 1$ and $\Delta_{\Uparrow\Downarrow}(\mathbf{k}) = -\Delta_S(\mathbf{k}) = -\Delta_{\Downarrow\Uparrow}(\mathbf{k})$ for helicity projection $\lambda = 0$. The amplitudes $\Delta_T(\mathbf{k}) = \Delta_0 |h_{\mathrm{ERD}}(\mathbf{k})|/|\mathbf{h}_{\mathrm{eff}}(\mathbf{k})|$ and $\Delta_S(\mathbf{k}) = \Delta_0 h_z/|\mathbf{h}_{\mathrm{eff}}(\mathbf{k})|$ reflect the triplet and singlet components of the OP in the helicity basis, respectively. The Bloch-sphere relation $|\Delta_T(\mathbf{k})|^2 + |\Delta_S(\mathbf{k})|^2 = |\Delta_0|^2$ shows that the singlet and triplet channels in the helicity basis are not independent.

Higher angular momentum pairing.—In the triplet terms, $\Delta_{\Uparrow\Uparrow}(\mathbf{k})$ and $\Delta_{\Downarrow\Downarrow}(\mathbf{k})$ contain not only p-wave, but also f-wave and higher odd partial waves, as seen from a multipole expansion of $|\mathbf{h}_{\mathrm{eff}}(\mathbf{k})|^{-1} = [h_z^2 + h_{\mathrm{ERD}}^2(\mathbf{k})]^{-1/2}$ for finite h_z. Similarly, in the singlet sector, $\Delta_{\Uparrow\Downarrow}(\mathbf{k})$ and $\Delta_{\Downarrow\Uparrow}(\mathbf{k})$ contain s-wave, d-wave, and higher even partial waves, as long as h_z is nonzero. Higher angular momentum pairing occurs because the local (zero ranged) interaction in the $(\uparrow, \downarrow)$ spin basis is transformed into a finite-ranged anisotropic interaction in the helicity basis $(\Uparrow, \Downarrow)$.

Excitation spectrum.—The effective Hamiltonian in the helicity basis takes the matrix form

$$\tilde{\mathbf{H}}_{\mathrm{sp}}(\mathbf{k}) = \begin{pmatrix} \xi_\Uparrow(\mathbf{k}) & 0 & \Delta_{\Uparrow\Uparrow}(\mathbf{k}) & \Delta_{\Uparrow\Downarrow}(\mathbf{k}) \\ 0 & \xi_\Downarrow(\mathbf{k}) & \Delta_{\Downarrow\Uparrow}(\mathbf{k}) & \Delta_{\Downarrow\Downarrow}(\mathbf{k}) \\ \Delta^*_{\Uparrow\Uparrow}(\mathbf{k}) & \Delta^*_{\Downarrow\Uparrow}(\mathbf{k}) & -\xi_\Uparrow(\mathbf{k}) & 0 \\ \Delta^*_{\Uparrow\Downarrow}(\mathbf{k}) & \Delta^*_{\Downarrow\Downarrow}(\mathbf{k}) & 0 & -\xi_\Downarrow(\mathbf{k}) \end{pmatrix}. \quad (2)$$

The eigenvalues for the highest and the lowest quasiparticle bands are $E^p_\pm(\mathbf{k}) = \sqrt{(|\mathbf{h}_{\mathrm{eff}}(\mathbf{k})| \pm \sqrt{K^2(\mathbf{k}) + |\Delta_S(\mathbf{k})|^2})^2 + |\Delta_T(\mathbf{k})|^2}$, while the eigenvalues for the quasihole bands are $E^h_\pm(\mathbf{k}) = -E^p_\pm(\mathbf{k})$. Note that $E^p_+(\mathbf{k}) > E^p_-(\mathbf{k}) \geq 0$, and only $E^p_-(\mathbf{k})$ can have zeros (nodal regions). The condition $E^p_-(\mathbf{k}) = 0$ corresponds physically to the equality between the effective magnetic field energy $|\mathbf{h}_{\mathrm{eff}}(\mathbf{k})|$ and excitation energy for the singlet component $\sqrt{K^2(\mathbf{k}) + |\Delta_S(\mathbf{k})|^2}$ and the vanishing of the triplet component of the OP $\Delta_T(\mathbf{k})$.

Phase diagram.—Since only $E^p_-(\mathbf{k})$ can have zeros, the low energy physics is dominated by this eigenvalue. In the ERD case, where $|h_{\mathrm{ERD}}(\mathbf{k})| = v|k_x|$, zeros can occur in $E^p_-(\mathbf{k})$ when $k_x = 0$, leading to the following cases: (a) two possible lines (rings) of nodes when $h_z^2 - |\Delta_0|^2 > 0$; (b) a doubly degenerate line of nodes for $\mu > 0$, a doubly degenerate point nodes for $\mu = 0$, or no line of nodes for $\mu < 0$ when $h_z^2 - |\Delta_0|^2 = 0$; and (c) no line of nodes when $h_z^2 - |\Delta_0|^2 < 0$. In addition, case (a) can be refined into cases (a2), (a1), and (a0). In case of (a2), two rings indeed exist, provided that $\mu > \sqrt{h_z^2 - |\Delta_0|^2}$. However, the inner ring disappears when $\mu = \sqrt{h_z^2 - |\Delta_0|^2}$. In case of (a1), there is only one ring when $|\mu| < \sqrt{h_z^2 - |\Delta_0|^2}$. In case of (a0), the outer ring disappears at $\mu = -\sqrt{h_z^2 - |\Delta_0|^2}$, and for $\mu < -\sqrt{h_z^2 - |\Delta_0|^2}$ no rings exist.

To obtain the phase diagram, we self-consistently solve the OP $\partial\Omega_{\mathrm{sp}}/\partial|\Delta_0|^2 = 0$ and number $N = -(\partial\Omega_{\mathrm{sp}}/\partial\mu)_{T,V}$ equations, where $\Omega_{\mathrm{sp}} = -T\ln(\mathrm{Tr}\exp(-\tilde{\mathbf{H}}_{\mathrm{sp}}/T)) + V|\Delta_0|^2/g + \sum_{\mathbf{k}} K(-\mathbf{k})$ is the thermodynamic potential (see Supplemental Material [16]).

In Fig. 1, we show the zero temperature ($T = 0$) phase diagrams of h_z/ϵ_F versus $1/(k_F a_s)$ as well as P_{ind} versus $1/(k_F a_s)$ for $v/v_F = 0$ and $v/v_F = 0.28$. We label the uniform superfluid phases with zero, one, or two rings of nodes as US-0, US-1, and US-2, respectively. Nonuniform (NU) phases emerge in regions where the uniform phases

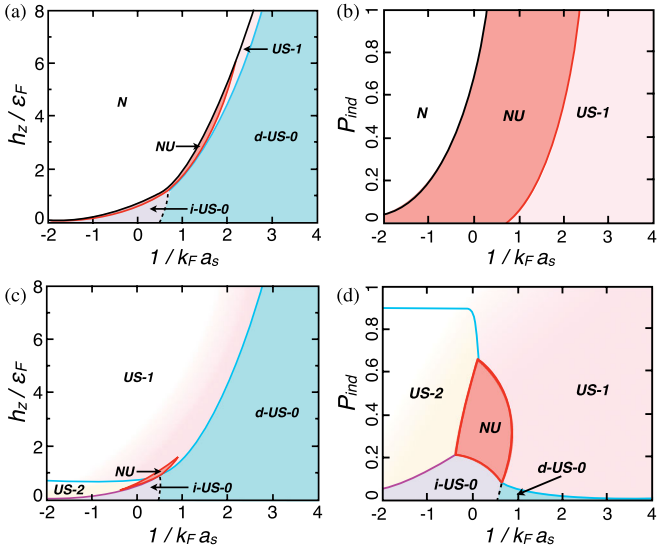

FIG. 1 (color online). Phase diagrams of h_z/ϵ_F and P_{ind} versus $1/(k_F a_s)$ for ERD coupling $v/v_F = 0$ (a), (b); and for ERD coupling $v/v_F = 0.28$ (c), (d). Uniform superfluid phases are labeled as US-0 (gapped, either directly or indirectly), US-1 (gapless with one ring of nodes), and US-2 (gapless with two rings of nodes). The NU label describes the region where uniform superfluids are unstable.

are thermodynamically unstable (see Supplemental Material [16]). The possible NU phases include phase separation, modulated superfluids, or supersolids. The phase boundary between US-2 and US-1 is determined by the condition $\mu = \sqrt{h_z^2 - |\Delta_0|^2}$, when $|h_z| > |\Delta_0|$; the US-0 or US-2 boundary is determined by the Clogston-like condition $|h_z| = |\Delta_0|$ when $\mu > 0$, where the gapped US-0 phase disappears leading to the gapless US-2 phase; and the phase boundary between US-0 and US-1 is determined by $\mu = -\sqrt{h_z^2 - |\Delta_0|^2}$, when $|h_z| > |\Delta_0|$. Furthermore, within the US-0 boundaries, a crossover between an indirectly gapped and a directly gapped phase occurs at $\mu = 0$.

Note that for finite SO coupling v, it is always possible to form pairs in the lower helicity band $\xi_{\Uparrow}(\mathbf{k})$, no matter how large h_z is, because an induced triplet component of the OP emerges and circumvents the standard pair—breaking Clogston limit for singlet pairing. The stable superfluid phase for a large h_z at $T = 0$ is the US-1 phase, as shown in Fig. 1 (see also Supplemental Material [16]).

Dirac and Majorana fermions.—Changes in nodal structures of excitation spectrum or the OP are associated with bulk topological phase transitions of the Lifshitz class, as noted for p-wave [17,18] and d-wave [19,20] superfluids. Such transitions are possible here because SO and Zeeman fields induce higher angular momentum pairing in the helicity basis. In the US-1 and US-2 phases near the zeros of $E_{-}^{p}(\mathbf{k})$, quasiparticles have linear dispersion and behave as Dirac fermions. The disappearance of nodal regions (rings) corresponds to annihilation of Dirac quasiparticles with opposite momenta. The transition from phase US-2 to indirect-gap i-US-0 occurs through the merger of the two rings at the phase boundary, followed by the immediate opening of the indirect gap at finite momentum. However, the transition from phase US-2 to US-1 corresponds to the disappearance of the inner ring through the origin of momenta ($\mathbf{k} = \mathbf{0}$), and the transition from phase US-1 to the direct-gap d-US-0 corresponds to the disappearance of the last ring, also through the origin of momenta.

The last two phase transitions (between US-2 and US-1, and between US-1 and d-US-0) are special, because the zero-momentum quasiparticles at these phase boundaries correspond to Majorana zero energy modes if the phase $\varphi(\mathbf{k})$ of the SO field $h_{\mathrm{ERD}}(\mathbf{k}) = |h_{\mathrm{ERD}}(\mathbf{k})|e^{i\varphi(\mathbf{k})}$, where $\varphi(\mathbf{k}) = \mathrm{sgn}(k_x)\pi/2$, and the phase $\theta(\mathbf{k})$ of the OP $\Delta_0 = |\Delta_0|e^{i\theta(\mathbf{k})}$ satisfy the relation at zero momentum: $\varphi(\mathbf{0}) = -\theta(\mathbf{0})[\mathrm{mod}(2\pi)]$. This can be seen from an analysis of the eigenfunctions $\Phi_i(\mathbf{k}) = U_{i1,\mathbf{k}}\psi_{\mathbf{k}\uparrow} + U_{i2,\mathbf{k}}\psi_{\mathbf{k}\downarrow} + U_{i3,\mathbf{k}}\psi^{\dagger}_{-\mathbf{k}\uparrow} + U_{i4,\mathbf{k}}\psi^{\dagger}_{-\mathbf{k}\downarrow}$, corresponding to the eigenvalue $E_{-}^{p,h}(\mathbf{k})$, where $U_{ij,\mathbf{k}} = \mathbf{U}_{ij}(\mathbf{k})$ are the elements of the unitary matrix $\mathbf{U}(\mathbf{k})$ that diagonalizes the Hamiltonian $\tilde{\mathbf{H}}_{\mathrm{sp}}(\mathbf{k})$. The emergence of zero-energy Majorana fermions requires the quasiparticle (quasihole) to be its own antiquasiparticle (antiquasihole): $\Phi_i^{\dagger}(\mathbf{k}) = \Phi_i(\mathbf{k})$. This happens at zero momentum $\mathbf{k} = \mathbf{0}$, where the amplitudes $U_{i1,\mathbf{0}} = U^{*}_{i3,\mathbf{0}}$ and $U_{i2,\mathbf{0}} = U^{*}_{i4,\mathbf{0}}$, leading to the conditions $\mu^2 = h_z^2 - |\Delta_0|^2$ and $\varphi(\mathbf{0}) = -\theta(\mathbf{0})[\mathrm{mod}(2\pi)]$. This shows that Majorana fermions exist only at the phase boundaries between US-1 and US-0 and between US-2 and US-1. In Fig. 2, we show the Lifshitz transition from US-1 to US-0 phase, where nodal (massless) Dirac fermions in the US-1 phase become bulk zero-mode Majorana fermions at the phase boundary between US-1 and US-0, and then become massive Dirac fermions in the US-0 phase.

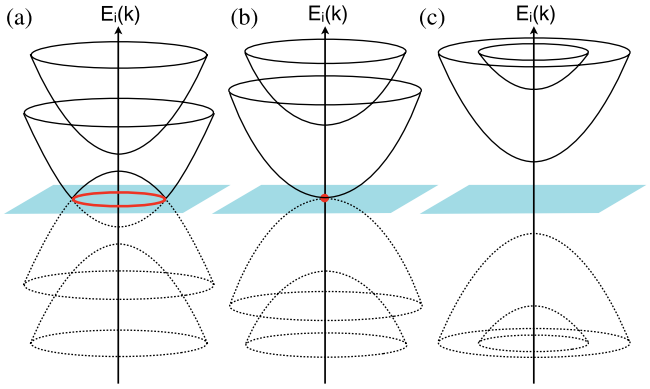

FIG. 2 (color online). Excitation spectra $E_i(\mathbf{k})$ in the ($k_x = 0$, k_y, k_z) plane illustrating the Lifshitz transition: the shrinkage of (a) Dirac rings (US-1 phase) into (b) Majorana zero-energy modes (phase boundary between US-1 and US-0) and (c) the emergence of massive Dirac fermions (direct-gap d-US-0 phase).

It is important to emphasize that the Majorana fermions found here are not the zero-energy Andreev bound states supposed to exist in junctions between one-dimensional quantum wires [21,22], and are not related to the zero-energy bound states expected to exist inside the vortex cores of $p_x + ip_y$ superfluids. The Majorana states found here are present in the bulk and are unbound zero-energy states, which happen to have zero momentum. Our Majorana mode can be expressed in terms of a linear combination of plane-wave states, as defined by the operator $\Phi_i(\mathbf{k})$. Such self-adjoint states are much closer to those originally envisioned by Majorana, and the work performed here (with small modifications) opens a path for finding finite-momentum bulk Majorana quasiparticles. The only commonality between the bulk (unbound) Majorana fermions found here and the bound-state Majorana fermions corresponding to zero-energy Andreev bound states found in junctions of topological superconductors is that both exist at boundaries: bulk Majorana zero-energy modes may exist at the phase boundaries between two topologically distinct superfluid phases, while bound-state Majorana zero-energy modes may exist at the spatial boundaries (junctions) between topologically nontrivial superconductors (see Supplemental Material [16]).

Lifshitz transition.—Transitions between different superfluid phases occur without a change in the symmetry of the OP tensor $\Delta_{\alpha\beta}(\mathbf{k})$ in the helicity basis, and thus violate the symmetry-based Landau classification of

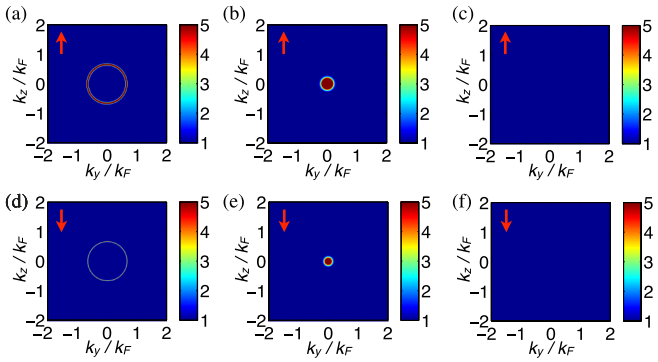

FIG. 3 (color online). The zero-energy spectral density $\mathcal{A}_s(\omega = 0, k_x = 0, k_y, k_z)$ at $1/(k_F a_s) = 1.0$ and $v/v_F = 0.28$ is shown in (a) and (d) for the US-1 phase with $h_z/\epsilon_F = 1.75$, in (b) and (e) for the phase boundary between US-1 and US-0 with $h_z/\epsilon_F = 1.59$, and in (c) and (f) for the direct-gap d-US-0 phase with $h_z/\epsilon_F = 1.44$. The top panels (a), (b), and (c) show $\mathcal{A}_\uparrow$, while the bottom panels (d), (e), and (f) show $\mathcal{A}_\downarrow$.

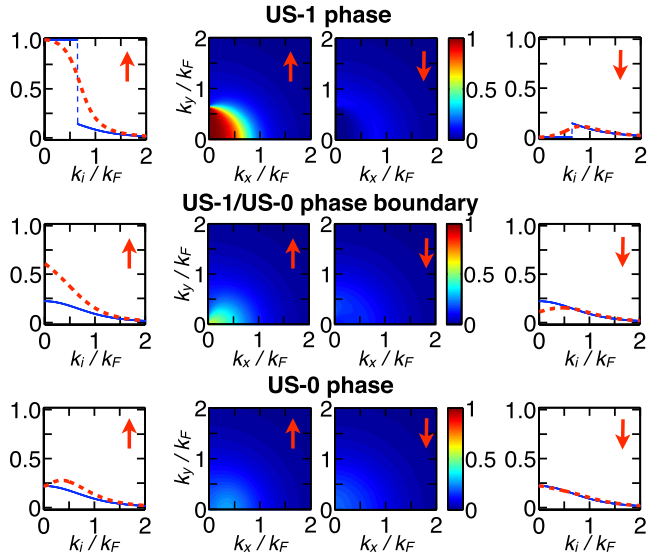

FIG. 4 (color online). Momentum distribution $n_s(\mathbf{k})$ for $1/(k_F a_s) = 1.0$ and $v/v_F = 0.28$ at the US-1 phase with $h_z/\epsilon_F = 1.75$ (top panels), at the US-1/US-0 phase boundary with $h_z/\epsilon_F = 1.59$ (middle panels), and at the US-0 phase with $h_z/\epsilon_F = 1.44$ (lower panels). The leftmost (rightmost) panels show the momentum distribution for spin $\uparrow$ ($\downarrow$) at $k_z = 0$ versus k_y (solid-blue line) and versus k_x (dotted-red line).

phase transitions. However, a finer classification based on topological charges can be made via the construction of topological invariants [17,23]. The number of rings ℓ corresponds to the topological charge associated with the surfaces of zero-energy quasiparticle excitations. Thus, for the US-0 phase $\ell = 0$, while for the US-1 and US-2 phases, $\ell = 1$ and $\ell = 2$, respectively.

Spectral function.—An important measurable quantity is the single-particle spectral density [24] $\mathcal{A}_s(\omega, \mathbf{k}) = -(1/\pi)\mathrm{Im}\mathbf{G}_{ss}(i\omega = \omega + i\delta, \mathbf{k})$ for spin $s = \uparrow, \downarrow$, where $\mathbf{G}(i\omega, \mathbf{k}) = (i\omega\mathbf{1} - \tilde{\mathbf{H}}_{\mathrm{sp}}(\mathbf{k}))^{-1}$. The existence of rings of zero-energy excitations for the US-1 and US-2 phases is revealed by the function $\mathcal{A}_s(\omega = 0, k_x = 0, k_y, k_z)$. In Fig. 3, the spectral densities for the US-1 phase are shown in the left panels (a) and (d). The ring for spin $\uparrow$ (a) is brighter than the ring for spin $\downarrow$ (d), since $P_{\mathrm{ind}} > 0$. In the middle panels (b) and (e), $\mathcal{A}_s(\omega = 0, k_x = 0, k_y, k_z)$ at the phase boundary between US-1 and US-0 is shown revealing the Majorana zero-energy mode. In the right panels (c) and (f), the spectral densities for the US-0 phase is zero at $\omega = 0$, since this phase is fully gapped.

Momentum distribution.—A spectroscopic quantity that is routinely measured is the momentum distribution $n_s(\mathbf{k}) = T\sum_{i\omega}\mathbf{G}_{ss}(i\omega, \mathbf{k})$ for spin $s = \uparrow, \downarrow$. Since $n_s(\mathbf{k})$ depends only on the energy spectrum $E^{p,h}_{\pm}(\mathbf{k})$ and its derivatives, it is an even function of momentum $\mathbf{k}$ (Fig. 4). It is very important to note the discontinuity of $n_s(\mathbf{k})$ at the location of the ring of zero-energy excitations in the US-1 phase (top panels), its change in behavior as bulk Majorana fermions emerge at $\mathbf{k} = 0$ (middle panels), and the transition to a direct-gap d-US-0 phase (bottom panels), where the ring of the nodes has disappeared, leading to smooth momentum distributions $n_s(\mathbf{k})$.

Trap effects.—Since we are dealing with ERD SO coupling, no angular momentum is injected into the system, and therefore the spontaneous emergence of vortices as in the case of Bose systems with Rashba-only or Dresselhaus-only SO coupling [25] does not occur. Therefore, vortex states due to the interplay of time-reversal symmetry breaking, SO coupling, and the trapping potential are not expected in the ERD case. However, an interesting effect due to the presence of the trapping potential is the coexistence of various superfluid regions. Since the system is inhomogeneous in a trap, the bulk Majorana states become now interface states. For instance, in the case of the phase boundary between US-2 and US-1, the Majorana states now occur when $\mu(\mathbf{r}) = \sqrt{h_z^2 - |\Delta_0(\mathbf{r})|^2}$, within the local density approximation $\mu(\mathbf{r}) = \mu - V_{\mathrm{tr}}(\mathbf{r})$ (see Supplemental Material [16]), and define a spherical shell when the trapping potential $V_{\mathrm{tr}}(\mathbf{r})$ is harmonic and spherically symmetric.

Summary.—We showed that the presence of simultaneous Zeeman and SO fields induces higher angular momentum pairing in the helicity basis. We have also identified topological phase transitions of the Lifshitz class via the existence of rings of nodes in the excitation spectra, Dirac quasiparticles, bulk Majorana zero-energy modes, and topological charges. Lastly, we characterized different topological phases and the emergence of bulk Majorana and Dirac fermions via experimentally measurable quantities such as the excitation spectrum, spectral function, and momentum distribution.

We thank ARO (W911NF-09-1-0220) for support.

[1] Y.-J. Lin, K. Jimenez-Garcia, and I. B. Spielman, Nature (London) **471**, 83 (2011).
[2] X.-J. Liu, M. F. Borunda, X. Liu, and J. Sinova, Phys. Rev. Lett. **102**, 046402 (2009).
[3] M. Chapman and C. Sá de Melo, Nature (London) **471**, 41 (2011).
[4] C. L. Kane and E. J. Mele, Phys. Rev. Lett. **95**, 146802 (2005).
[5] L. P. Gor'kov and E. I. Rashba, Phys. Rev. Lett. **87**, 037004 (2001).
[6] T. D. Stanescu, C. Zhang, and V. Galitski, Phys. Rev. Lett. **99**, 110403 (2007).
[7] E. I. Rashba, Sov. Phys. Solid State **2**, 1109 (1960).
[8] J. P. Vyasanakere, S. Zhang, and V. B. Shenoy, Phys. Rev. B **84**, 014512 (2011).
[9] M. Gong, S. Tewari, and C. Zhang, Phys. Rev. Lett. **107**, 195303 (2011).
[10] Z.-Q. Yu and H. Zhai, Phys. Rev. Lett. **107**, 195305 (2011).
[11] H. Hu, L. Jiang, X.-J. Liu, and H. Pu, Phys. Rev. Lett. **107**, 195304 (2011).
[12] M. Iskin and A. L. Subasi, Phys. Rev. Lett. **107**, 050402 (2011).
[13] L. Han and C. A. R. Sá de Melo, Phys. Rev. A **85**, 011606 (R) (2012).
[14] G. Dresselhaus, Phys. Rev. **100**, 580 (1955).
[15] J. Dalibard, F. Gerbier, G. Juzeliūnas, and P. Öhberg, Rev. Mod. Phys. **83**, 1523 (2011).
[16] See Supplemental Material at http://link.aps.org/supplemental/10.1103/PhysRevLett.109.105303 for details about the helicity basis, self-consistency relations, thermodynamic stability and trap effects.
[17] G. E. Volovik, *Exotic Properties of Superfluid* ^{3}He (World Scientific, Singapore, 1992).
[18] S. S. Botelho and C. A. R. Sá de Melo, J. Low Temp. Phys. **140**, 409 (2005).
[19] R. D. Duncan and C. A. R. Sá de Melo, Phys. Rev. B **62**, 9675 (2000).
[20] S. S. Botelho and C. A. R. Sá de Melo, Phys. Rev. B **71**, 134507 (2005).
[21] R. M. Lutchyn, J. D. Sau, and S. Das Sarma, Phys. Rev. Lett. **105**, 077001 (2010).
[22] Y. Oreg, G. Refael, and F. von Oppen, Phys. Rev. Lett. **105**, 177002 (2010).
[23] M. Nakahara, *Geometry, Topology and Physics* (Adam Hilger, Bristol, 1990).
[24] J. P. Gaebler, J. T. Stewart, T. E. Drake, D. S. Jin, A. Perali, P. Pieri, and G. C. Strinati, Nature Phys. **6**, 569 (2010).
[25] S. Sinha, R. Nath, and L. Santos, Phys. Rev. Lett. **107**, 270401 (2011).